Available online at www.eccomasproceedia.org
Eccomas Proceedia COMPDYN (2023) 3157-3172

ECCOMAS
Proceedia

COMPDYN 2023
9th ECCOMAS Thematic Conference on
Computational Methods in Structural Dynamics and Earthquake Engineering
M. Papadrakakis, M. Fragiadakis (eds.)
Athens, Greece, 12-14 June 2023

THE INFLUENCE OF DAMPING ON PROGRESSIVE COLLAPSE ANALYSIS

Alex S. Cao[1] **and Andrea Frangi**[2]

[1]Institute of Structural Engineering, ETH Zurich
Stefano-Franscini-Platz 5, 8093 Zurich, Switzerland
e-mail: cao@ibk.baug.ethz.ch

[2] Institute of Structural Engineering, ETH Zurich
Stefano-Franscini-Platz 5, 8093 Zurich, Switzerland
e-mail: frangi@ibk.baug.ethz.ch

Abstract. *The most common method of modeling damping in structures is with equivalent viscous damping with the Rayleigh damping model. However, it is well-known that the Rayleigh damping model may cause spurious damping forces and nonphysical behavior for inelastic structures. Remedies have been proposed to overcome these problems, such as various incremental versions using the tangent stiffness or the use of modal damping instead. These may be appropriate for inelastic structures with negligible changes of the vibration modes, and without softening behavior for the Rayleigh damping models. In progressive collapse analyses, these damping models may be inappropriate because of the radical change in vibration modes, as well as the changes to the mass and stiffness matrix. In this paper, initial and incremental versions of the Rayleigh and modal damping models are presented and compared for a structure undergoing progressive collapse. The damping model is not critical if the objective is to assess the response until the first failure. However, the choice of the damping model may lead to large dissimilarities after the first failure in a progressive collapse analysis.*

Keywords: Equivalent Viscous Damping, Rayleigh Damping, Modal Damping, Structural Dynamics, Progressive Collapse, Nonlinear Response History Analysis.

ISSN:2623-3347
Peer-review under responsibility of the organizing committee of COMPDYN 2023.
doi: 10.7712/120123.10630.20674

1 INTRODUCTION

Nonlinear response history analysis is a versatile tool that can be used in performance-based design [1] and to simulate the response of structures subjected to various dynamic loading, such as earthquake loading [1], wind loading [2], blast and impact loading [3, 4], and progressive collapse [5]. The nonlinearities in nonlinear response history analysis may stem from large deformations, inelastic material behavior, and more. An important consideration for the dynamic response of a structure is the amount of damping and its model implementation.

For inelastic structures, the damping would ideally be modeled explicitly in the model as the hysteresis of the different materials [6]. This supposes that the hysteresis of the different materials used in the model is known, which may not be trivial. Besides, implementing hysteresis directly in the model as distributed or concentrated plasticity quickly leads to a bottleneck in terms of computational expenses for the analysis. A common alternative to the explicit modeling of hysteresis in the model is the use of equivalent viscous damping with the Rayleigh damping model or other damping models. A combination of equivalent viscous damping and the explicit modeling of hysteresis in the materials can also be used.

The advantage of using equivalent viscous damping is its computational efficiency in comparison with the direct modeling of hysteresis. For elastic structures or structures with moderate inelastic behavior, the use of equivalent viscous damping may result in acceptable results. However, the use of common damping models with equivalent viscous damping for strongly inelastic structures with large deformations may lead to large non-physical or spurious damping forces. This problem is particularly pronounced in Rayleigh damping [1, 6, 9]. Besides, equivalent viscous damping is often measured for structures in their elastic range [1] and it may not reflect the damping for inelastic structures [7].

To overcome the problems related to conventional Rayleigh damping, several researchers have suggested to use the tangent stiffness in Rayleigh damping [6, 8]. Another approach is to keep the calibration parameters in Rayleigh damping constant throughout the analysis [6]. Other alternative damping models are mass-proportionate damping [8], capped damping [10], modal damping [1, 11], and more.

In progressive collapse analysis, structures typically undergo large deformations and exhibit strong inelastic behavior. The failure and subsequent detachment and loss of structural members lead to changes in the remaining structure's stiffness and mass matrices. The loss of members also affects the damping properties of the structure. For damping models which rely on a combination of the initial stiffness and mass matrices to form the damping matrix, spurious damping forces are a certainty. Besides the spurious damping forces, the unchanged damping matrix may lead to convergence problems and a loss of computational efficiency associated with classical damping models.

This paper presents different variations of initial and incremental Rayleigh damping, as well as initial and incremental modal damping and their appropriateness for progressive collapse analysis. The performance of the different damping models is compared in a case study of a symmetric timber frame with four bays and four stories. Progressive collapse is introduced through the dynamic removal of an edge column, and the collapse is simulated using a recently developed collapse model [12]. The collapse model is parametric and includes element separation and detachment [13], element-removal [14], impact loading [15], and various damping models. The timber frame comprises glued laminated timber beams and columns, and laterally loaded timber connections with dowel-type fasteners and slotted-in steel plates. To find the equivalent viscous damping, a newly developed multi-scale hysteretic connection model is

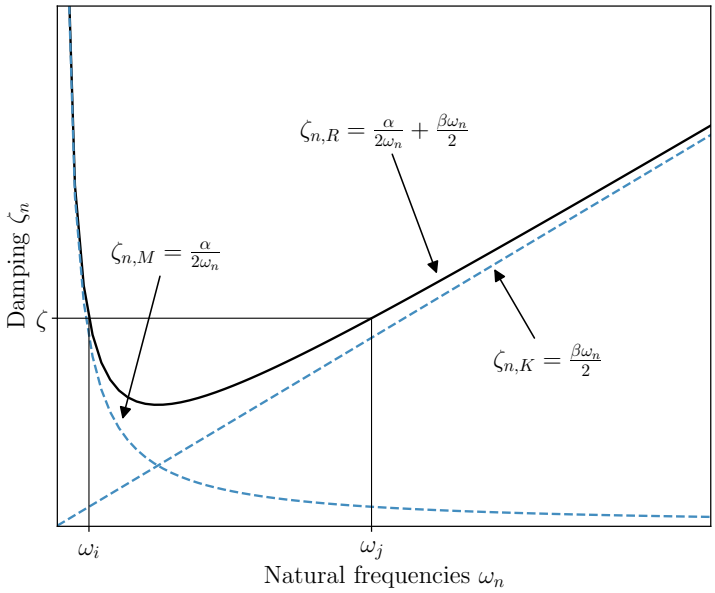

Figure 1: Damping ζ_n of frequency ω_n in Rayleigh damping.

used [16]. With the resulting hysteresis, a secant stiffness approach is used to model the frame connections.

2 DAMPING MODELS

In this paper, the Rayleigh damping and modal damping models were investigated. Rayleigh damping was assessed in its initial and incremental form, with initial and incremental calibration parameters. Similarly, modal damping was assessed in its initial and incremental form. The following subsections present the different damping models.

2.1 Rayleigh damping

In Rayleigh damping, the damping matrix $\mathbf{c}$ is a linear combination of the stiffness $\mathbf{k}$ and mass $\mathbf{m}$ matrices:

$$\mathbf{c} = \alpha\mathbf{m} + \beta\mathbf{k}, \tag{1}$$

where α and β are calibration parameters. If the damping ratio ζ is constant throughout all the modes, the calibration parameters α and β are:

$$\begin{aligned} \alpha &= 2\zeta\frac{\omega_i\omega_j}{\omega_i + \omega_j}, \\ \beta &= 2\zeta\frac{1}{\omega_i + \omega_j}, \end{aligned} \tag{2}$$

where ω_i and ω_j are the angular frequencies that the calibration parameters α and β are computed for. The angular frequencies ω_i and ω_j often inherit the values of the first and a higher frequency mode of a structure, which are picked based on their importance for the dynamic response of the structure. With the calibration factors in Equation 2, it is assumed that the damping ζ is the same for frequency ω_i and ω_j.

2.1.1 Initial Rayleigh

In the most common implementation of Rayleigh damping, an eigenvalue analysis is conducted before the dynamic analysis, and the damping matrix **c** is computed from the resulting eigenvalues at the initial state of the structure. In this paper, this approach is referred to as initial Rayleigh damping. Initial Rayleigh damping may lead to spurious or non-physical damping forces $\mathbf{f}_D = \mathbf{c}\dot{\mathbf{u}}$ for inelastic structures, where $\dot{\mathbf{u}}$ is the velocity [1, 6, 9, 10]. Besides, the results may not be conservative in a nonlinear response history analysis [11].

The root cause of the spurious damping forces $\mathbf{f}_D$ lies in the formulation of the Rayleigh damping model, which includes a contribution from the stiffness matrix **k**. For a certain displacement **u** of a structure, the resulting forces $\mathbf{f}_S = \mathbf{k}\mathbf{u}$ of a linear-elastic idealization would be larger than the real response of the structure in the inelastic range, where hardening or softening may be present and the actual stiffness **k** of the system may be lower. In initial Rayleigh damping, the stiffness contribution **k** does not change. This results in an increasing error from initial Rayleigh damping with the magnitude of inelasticity experienced by the structure.

Besides the spurious damping forces $\mathbf{f}_D$ that stem from the constant stiffness contribution $\mathbf{c}_k = \beta\mathbf{k}$, the inertia forces $\mathbf{f}_I = \mathbf{m}\ddot{\mathbf{u}}$ and the velocity $\dot{\mathbf{u}}$ may also encounter problems. If there is a change in the stiffness **k**, this implies that the natural frequency $\omega_n = \lambda_n\sqrt{k/m}$ would also change. If the structure experiences hardening or softening, the natural frequency ω_n would become smaller because of the reduced stiffness **k**. Consequently, the natural period T_n would become longer and the velocity $\dot{\mathbf{u}}$ and acceleration $\ddot{\mathbf{u}}$ would be reduced. This would lead to a direct reduction in the inertia $\mathbf{f}_I$ and damping forces $\mathbf{f}_D$ as well. However, a linear-elastic idealization with initial Rayleigh damping cannot replicate this behavior for inelastic systems.

In the analysis of the progressive collapse of structures with elastic or inelastic material behavior, the use of initial Rayleigh may cause larger spurious damping forces. Suppose that a model can simulate a progressive collapse, including the separation and detachment of members upon failure. If the members of the structure have linear-elastic perfectly brittle materials, then the structure will only experience a change in the stiffness **k** and mass **m** matrices as the different members fail, separate, and detach from the remaining structure. Initial Rayleigh damping cannot reflect these changes, as the damping matrix **c** is computed from the initial stiffness **k** and mass **m** matrices. Therefore, initial Rayleigh damping results in an increasing amount of spurious damping forces $\mathbf{f}_D$ as more and more members fail during the progressive failure. Besides, the equation solving becomes inefficient and convergence problems may ensue as the damping matrix **c** retains non-zero entries for elements that are removed.

2.1.2 Incremental Rayleigh

To overcome the problem of spurious damping forces in initial Rayleigh damping, several remedies have been proposed. A common approach is to replace the initial stiffness in initial Rayleigh damping with the tangent stiffness, which is updated incrementally [6, 8, 10]. Here, this approach is slightly modified and is referred to as incremental Rayleigh damping, where both the stiffness **k** and mass **m** matrices are updated at each time-step. There are several variations of incremental Rayleigh damping, where the calibration factors in Equation 2 may be computed only once, or incrementally [1, 6, 8, 10]. This can also be combined with the tangent stiffness.

In progressive collapse analysis, the use of incremental Rayleigh damping solves some problems related to initial Rayleigh damping. To a certain extent, it also solves the problems related

to spurious damping forces for inelastic structures. However, the updating of the stiffness matrix $\mathbf{k}$ may lead to an unstable response if the structure experiences softening behavior. If softening behavior is present in the structure, the stiffness matrix $\mathbf{k}$ may become negative. This implies that the damping matrix $\mathbf{c}$ in Equation 1 may decrease and eventually become negative. Consequently, the damping force $\mathbf{f}_D$ may transition from being a resisting force to an exerting force. Therefore, the structure's vibrations may grow uncontrollably. Besides the aforementioned problems, it may also become impossible to find real-valued positive eigenvalues because of the negative stiffness matrix $\mathbf{k}$.

A physical interpretation of the growing vibrations is that the structure experiences an influx of energy from the work exerted on the structure from the negative damping force $\mathbf{f}_D$. This exerted work must materialize in kinetic or strain energy in the structure, which results in larger response amplitudes to accommodate the additional energy. Unless the structure is subjected to an external force, this mechanism is physically impossible. Therefore, incremental Rayleigh damping can only be used for structures which do not experience softening behavior.

Besides the aforementioned problems with incremental Rayleigh, there is another worrying property. Because incremental Rayleigh damping changes with the state of the stiffness matrix $\mathbf{k}$, the damping of a monotonically loaded structure may be accurate. If, however, the structure experiences an inelastic response with hysteresis, the stiffness matrix $\mathbf{k}$ will change throughout the hysteretic response. Consequently, the damping force $\mathbf{f}_D$ would inherit the hysteresis of the stiffness matrix $\mathbf{k}$. Because most vibration measurements are conducted for structures in their elastic range, it is largely unknown whether damping should have the property of hysteresis [1].

2.2 Modal damping

As an alternative to Rayleigh damping, modal damping can be used [1]. In modal damping, the damping matrix $\mathbf{c}$ is defined as a superposition of modal damping matrix contributions:

$$\mathbf{c} = \mathbf{m}\left(\sum_{n=1}^{N} \frac{2\zeta_n\omega_n}{M_n}\phi_n\phi_n^T\right)\mathbf{m}, \tag{3}$$

where ζ_n is the damping ratio, ω_n is the natural angular frequency, M_n is the generalized mass, and ϕ_n is the eigenvector for mode n. The generalized mass matrix is defined as $\mathbf{M} = \Phi^T\mathbf{m}\Phi$, where Φ is the modal matrix. The generalized mass matrix $\mathbf{M}$ is a diagonal matrix comprising M_n diagonal entries.

2.3 Initial modal damping

For the modal damping matrix in Equation 3, damping contributions of N modes are included. If the modal damping matrix $\frac{2\zeta_n\omega_n}{M_n}\phi_n\phi_n^T$ from mode n is not included, there is no damping $\mathbf{c}$ in this mode. To ensure that the response of the system is accurate, a sufficient number of modes N must be included in the analysis.

Similarly to initial Rayleigh damping, modal damping computed for the initial elastic state may cause spurious damping forces $\mathbf{f}_D$ for inelastic structures. One of the main assumptions of modal analysis is that the structural response is linear and subjected to small deformations. Because the different parameters of modal damping in Equation 3 relies on solving the eigenvalue problem $\det\left[\mathbf{k} - \omega_n^2\mathbf{m}\right] = 0$ in modal analysis, their accuracy may be in question for the inelastic response of a structure with large deformations.

However, initial modal damping will not result in a negative damping matrix $\mathbf{c}$ and damping force $\mathbf{f}_D$ in most cases, as the eigenvalues of a structure ω_n^2 are mostly non-negative in the elas-

tic state. Negative eigenvalues ω_n^2 are physically plausible if a structure experiences dynamic buckling or snap-through. However, most cases of negative eigenvalues ω_n^2 are associated with modeling errors and are not physically plausible. This is especially true for an eigenvalue analysis conducted for a structure in the elastic state.

Using initial modal analysis is less problematic than the different variations of Rayleigh damping. For the inelastic response of structures, initial modal damping offers superior performance compared with Rayleigh damping [1, 11]. For progressive collapse analysis, initial modal damping is fraught with similar challenges as incremental Rayleigh damping because of the changing mass **m** and stiffness **k** during a progressive collapse. The changing mass **m** and stiffness **k** leads to changes in the natural angular frequencies ω_n and the eigenvectors ϕ_n, which affects the damping matrix **c** in Equation 3 directly.

2.4 Incremental modal damping

A remedy for overcoming the shortcomings of initial modal damping, is its incremental alternative. If a sufficiently small time-step Δt is used in a dynamic analysis, the structural response between time t_i and t_{i+1} may be considered linear and the deformations may be small. Therefore, updating the modal damping incrementally throughout an analysis may better reflect the real response of a structure in its inelastic state.

A disadvantage of incremental modal damping is the need to conduct an eigenvalue analysis at each time t_i. For small models with a few degrees of freedom, this may be unproblematic. However, larger models will be substantially more computationally expensive in comparison with initial modal damping. To make the equation solving more efficient, the damping matrix **c** can be updated at every other time t_i, or the time-step Δt can be increased. The trade-off between computational efficiency and numerical accuracy should be quantified for every analysis with a sensitivity study.

Besides the computational expense of conducting an eigenvalue analysis at each time t_i, convergence problems may ensue because of the eigenvalue analysis. For initial modal damping, the occurrence of negative eigenvalues ω_n^2 is highly unlikely. However, a structure in its inelastic state may experience instabilities. These instabilities may occur because of changes in the stiffness matrix **k** from hardening or softening behavior. In progressive collapse analysis, or for structures subjected to extreme loading, the likelihood of instabilities is not negligible.

3 MATERIALS AND METHOD

3.1 Frame design

The frame was designed for gravity loads according to EN 1990:2002 [17] and EN 1991-1-1:2002 [18] with the following load combination:

$$p_{Ed} = \xi \gamma_G g_k + \gamma_Q q_k, \tag{4}$$

where ξ is 0.85, γ_G is 1.35, γ_Q is 1.50, g_k is 3.5 kN/m^2, and q_k is 3.0 kN/m^2. Glued laminated timber with a strength class of GL24h was chosen for the beams and columns. Characteristic material parameters were assumed from EN 14080:2013 [19], and the beams and columns were designed with EN 1995-1-1:2004 [20]. The beams were assumed to have simply supported boundary conditions, and the columns were assumed to be continuous. The frame also satisfied the serviceability criterion for wind-induced vibrations from ISO 10137:2007 [21], where the peak accelerations were computed with EN 1991-1-4:2005 Annex B [22]. For the wind-induced vibrations, an equivalent viscous damping ζ_{eq} of 0.02 was chosen.

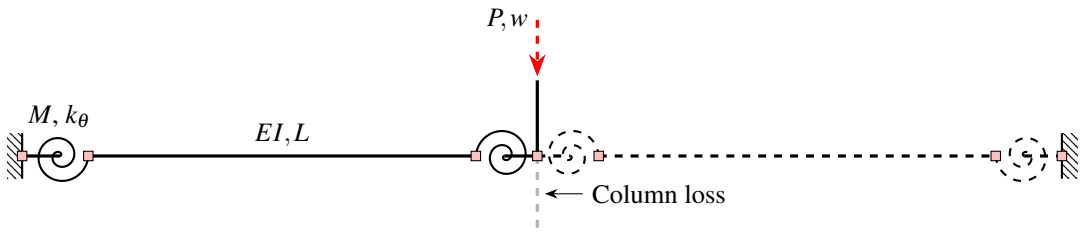

Figure 2: Structural system for the estimation of the equivalent viscous damping ζ_{eq}.

To connect the beams and the columns, laterally loaded timber connections with dowel-type fasteners were designed with EN 1995-1-1:2004 [20]. The connections comprised a single slotted-in steel plate and six dowel-type fasteners arranged in a 3×2 rectangular pattern with minimum distances specified in EN 1995-1-1:2004 [20]. The slotted-in steel plate had a thickness of 10 mm, and the dowels had a diameter of 10 mm. Both the slotted-in steel plate and the dowels were S235 steel with a characteristic yield strength $f_{y,k}$ of 235 N/mm^2 and an ultimate strength $f_{u,k}$ of 360 N/mm^2.

3.2 Equivalent viscous damping

To estimate the equivalent viscous damping ζ_{eq}, a multi-scale hysteretic model of laterally loaded timber connections with dowel-type fasteners [16] was used, with material parameters on the mean level [23, 24]. The multi-scale connection model was implemented for the simplified column-loss scenario in Figure 2, where it was assumed that the connections were subjected to a maximum rotation θ_u of $3\theta_y$, where θ_y is the yield rotation. For the connections in this paper, the yield rotation θ_y was 25.8 mrad, which corresponds to a maximum rotation θ_u of 77.5 mrad. If the beams are considered as rigid bodies, a maximum rotation θ_u of 77.5 mrad corresponds to approximately 279 mm in vertical deflections u_z of the node above the removed column.

The maximum rotation θ_u was used to simulate the hysteresis of the connection for a fully reversed displacement-controlled loading cycle of the structure in Figure 2. In Figure 3, the resulting hysteresis of the connection is shown. The total dissipated energy E_d was computed by integrating the area inside the envelope of the hysteresis, and the equivalent viscous damping ζ_{eq} was found from:

$$\zeta_{eq} = \frac{1}{4\pi}\frac{E_d}{E_s}, \tag{5}$$

where E_s is the strain energy calculated from the secant stiffness k_θ of the point of maximum rotation. With Equation 5 and a maximum rotation of $3\theta_y$, the equivalent viscous damping ζ_{eq} of the connection was 17.94%.

3.3 Simulations

For the simulations, a symmetrical frame with four bays and four storeys was chosen. The frame was subjected to the removal of an edge column. This is shown in Figure 4, with the removed column in red. The connections in Section 3.1 were idealized with a linear-elastic perfectly brittle material behavior. For the rotational stiffness k_θ of the connections, the secant stiffness of the maximum rotation θ_u of the hysteresis in Figure 5 was used, and the maximum rotation θ_u was used to define the brittle failure. The simulations were conducted with a recently developed parametric nonlinear model for progressive collapse analysis [12]. The model

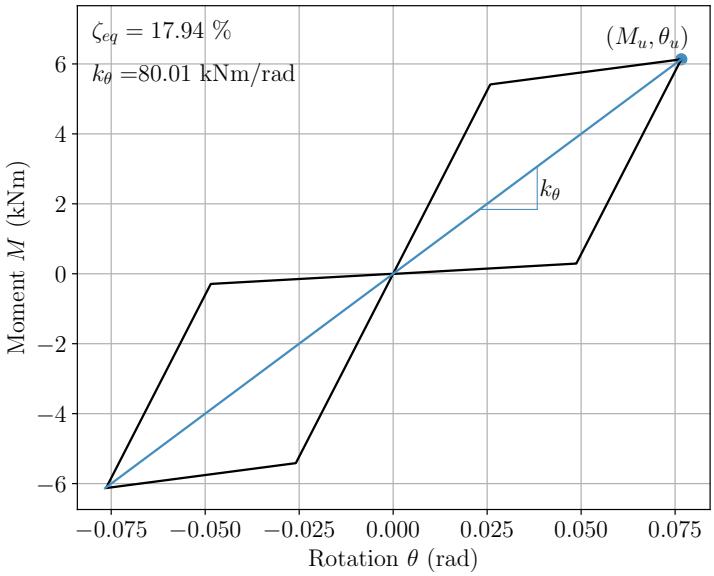

Figure 3: Hysteresis of the connection with a maximum rotation θ of $3\theta_y$, equivalent to 77.5 mrad. $k_{\theta,el}$ = 210 kNm/rad, $k_{\theta,pl}$ = 8.38 kNm/rad, $k_{\theta,sec}$ = 80.0 kNm/rad

Damping	α and β	**k**	**m**	Eigenvalues
Initial Rayleigh	Initial	Initial	Initial	Initial
Incremental Rayleigh	Constant	Incremental	Incremental	Incremental
Incremental Rayleigh	Incremental	Incremental	Incremental	Incremental
Initial modal	-	Initial	Initial	Initial
Incremental modal	-	Incremental	Incremental	Incremental

Table 1: Overview of the different methods. In the incremental Rayleigh with incremental α_t and β_t and initial Rayleigh with constant $\alpha_{t=0}$ and $\beta_{t=0}$ damping models, the first ω_1 and fifth ω_5 frequencies were used. For the incremental Rayleigh with constant $\alpha_{t=0}$ and $\beta_{t=0}$ damping model, the second calibration frequency ω_j in Equation 2 was $5\omega_1$.

includes features such as element removal, detachment of elements or structural assemblies, debris tracking, impact loading, and more.

In this paper, the different damping models described in Section 2 were investigated with an equivalent viscous damping ζ_{eq} of 17.94%. These are summarized in Table 1. For the initial Rayleigh damping and incremental Rayleigh damping with varying α_t and β_t parameters, the first ω_1 and fifth ω_5 modes were used for the damping matrix **c** in Equation 1. In the simulation with incremental Rayleigh damping with constant $\alpha_{t=0}$ and $\beta_{t=0}$, the frequencies ω_1 and $5\omega_1$ were used. For the modal damping models, analyses with 5, 10, and 20 modes N were conducted. In addition, $N = 30$ modes were also simulated for the incremental modal damping model. Ten simulations of edge column removals were performed.

To quantify the deviations between the models, the root-mean-square deviation RMSD and normalized root-mean-square deviation NRMSD were used, which can be expressed as:

$$\mathrm{RMSD}\left(y_{mn}\right) = \sqrt{\frac{\sum_{t=1}^{T}\left(y_{m,t} - y_{n,t}\right)^2}{T}}, \tag{6}$$

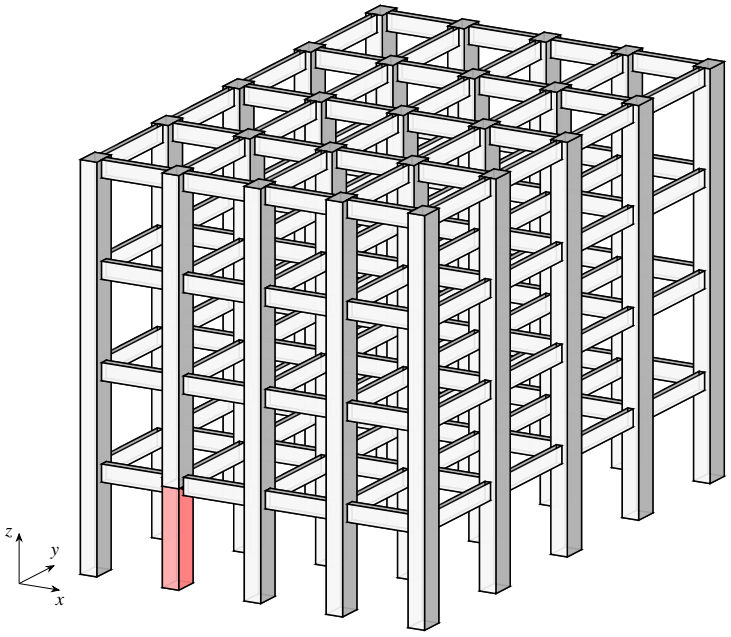

Figure 4: Structural system with the removed column in red.

$$\mathrm{NRMSD}\left(y_{mn}\right) = \frac{\mathrm{RMSD}}{\bar{y}_{mn}},$$

where y is a time series, indices m and n are two different time series, t is the time, T is the length of the time series, and $\bar{y}$ is the mean value of the time series. The normalized root-mean-square deviation NRMSD can be interpreted as the coefficient of variation cov of the compared time series, and the root-mean-square deviation RMSD as the standard deviation of the compared time series.

4 RESULTS AND DISCUSSION

4.1 Progressive collapse

Figure 5 shows the different damage states during the progressive collapse for the incremental modal damping model with $N = 20$ modes, with different nodes marked in Figure 5a. The course of the progressive collapse was similar for all the damping models. Following the removal of the column, node 4 deflected vertically to a deflection u_z of 276 mm in Figure 5a. This is similar to the deflection level of the calibrated equivalent viscous damping ζ_{eq}, presented in Section 3.2. Because of the large vertical deflections u_z and the corresponding rotations θ of the adjacent connections in the x-direction of the structure above the removed column, most of these beam-column connections failed. This is shown in Figure 5b and is referred to as the secondary damage state. In the tertiary damage state, the beam-column connections in the y-direction adjacent to the columns above the removed column failed. In the final damage state, the two bays sharing the removed column had collapsed.

For this structure, the progressive collapse was contained within two bays, with a collapsed floor area above ground of 78 m^2. This is equivalent to 12.5% of the total floor area and is less than the indicative limit of 100 m^2 or 15% in EN 1991-1-7:2006 [25]. The limited damage propagation can be attributed to the connections, which acted as fuse elements or weak links. The connections did not have a sufficient rotational capacity θ_u to activate alternative load paths through catenary action or vertical suspension of the structure adjacent to and above the re-

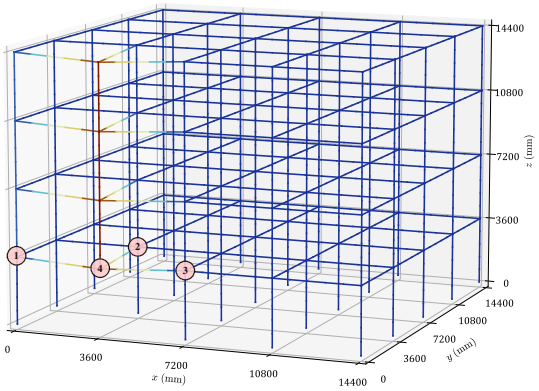

(a) Initial damage state with node numbering, $u_{z,\max} \simeq 276$ mm.

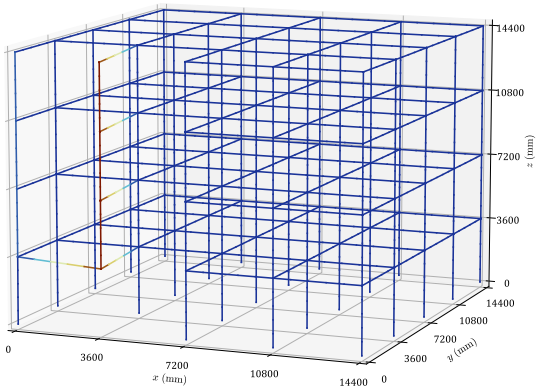

(b) Secondary damage state, $u_{z,\max} \simeq 277$ mm.

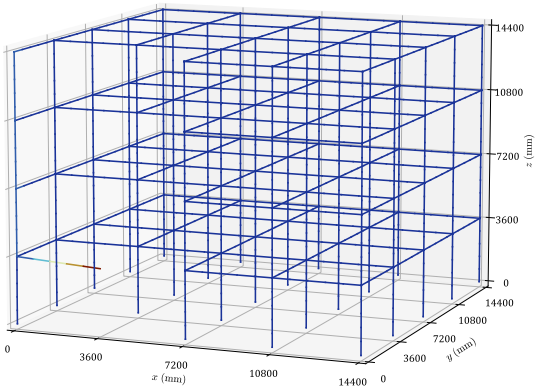

(c) Tertiary damage state, $u_{z,\max} \simeq 251$ mm.

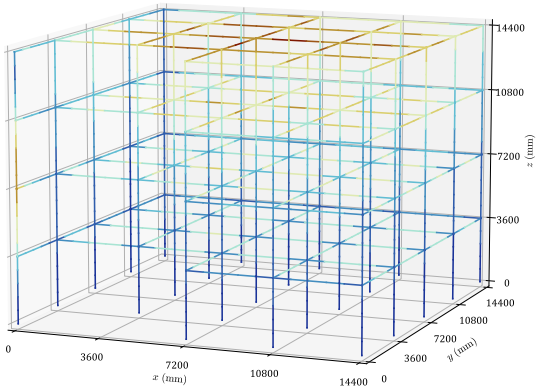

(d) Final damage state, $u_{z,\max} \simeq 10$ mm.

Figure 5: Damage states during the collapse.

moved column. Therefore, the collapse was limited to two bays. This is similar to the collapse of the Siemens arena [26]. With sufficient rotational capacity θ_u in the connections, alternative load paths could have developed, which might have led to the arrest of the collapse. Another scenario with an increased rotational capacity θ_u could be the propagation of collapse because of the absence of the fuse elements, similar to the collapse of the Bad Reichenhall ice-arena [26].

4.2 Convergence and computation time

The incremental Rayleigh model with incremental α_t and β_t had a computation time of 50 453 s on a desktop computer with an Intel Xeon CPU E3-1225 V2 @3.20 GHz processor run-

ning on a single core, which was approximately 4.4 % longer than the initial Rayleigh damping model. There was no significant difference in the computation time between the initial Rayleigh damping model and the incremental Rayleigh model, with constant $\alpha_{t=0}$ and $\beta_{t=0}$. Because the structural responses of the different Rayleigh models were practically identical, it is sensible to use the incremental Rayleigh model with constant $\alpha_{t=0}$ and $\beta_{t=0}$ for similar analyses.

For the initial modal damping model, the response histories of the simulations with $N = 10$ and $N = 20$ modes were similar for node ①. The dissimilarities were slightly larger for nodes ② and ③, where the displacement magnitudes were slightly different. The computation time for the initial modal damping model with $N = 20$ modes was 105 720 s. This was approximately 5.4% longer than with $N = 10$ modes. Because of the gain in accuracy when using $N = 20$ modes compared to $N = 10$ modes and the relatively small difference in computation time, it is sensible to use $N = 20$ modes for similar analyses. In the following discussion in Section 4.3, the results from the analyses with $N = 20$ modes are used.

For the incremental modal damping model, convergence was reached for $N = 30$ modes. This can be seen in Figure 6, where the response histories of the $N = 20$ and $N = 30$ modes were fairly similar. The computation time for the incremental modal damping model with $N = 30$ modes was 75 554 seconds, or about 14.5% longer than with $N = 20$ modes. Although the response history for nodes ① and ③ were almost identical, there was a larger discrepancy for node ②. Therefore, $N = 30$ modes should be used for similar analyses with the incremental modal damping model. In the following discussion in Section 4.3, the results from the analyses with $N = 30$ modes are used.

4.3 Comparison of damping models

For the different nodes in Figure 5a, the response histories of the different damping models are shown in Figure 6. The response histories of the different variations of Rayleigh damping and initial modal damping models were quite similar for nodes ①, ②, and ③. Although all models resulted in the same oscillation trends, the magnitudes of the peaks for the incremental modal damping model were severely dissimilar from the other damping models. The maximum deformations for nodes ① to ③ with the incremental damping models were approximately five times higher than for the other damping models, and the peak deformations occurred later.

The Rayleigh variations and the initial modal damping models damped out higher-mode response, which can be seen from the relatively smooth curves in Figure 6. For initial modal damping with $N = 5$ modes, higher mode response was also present. However, the higher mode response became less pronounced as more modes N were included in the damping matrix $\mathbf{c}$ in Equation 3. For the incremental modal damping model, higher mode response was much more pronounced. This can be seen from the ruggedness of the curves, especially for nodes ② and ③ after $t = 0.5$ s. Although higher mode response was captured better in the incremental modal damping model, its significance in progressive collapse simulations may be limited as long as the displacement magnitudes are correctly represented.

Figure 6d shows the response history of node ④ for the different damping models. The different Rayleigh and modal damping models result in almost identical response histories with similar failure points. If the objective of the analyses are to model the initial failure, the choice between the different damping models in this paper is not important, as the shape of the response history and the failure points are fairly similar. If the objective of the analyses is to assess the response of the structure past the first failure, the choice of the damping model is important. This can be seen in Figures 6a-c, with the large deviations between the incremental modal damping model and the other damping models.

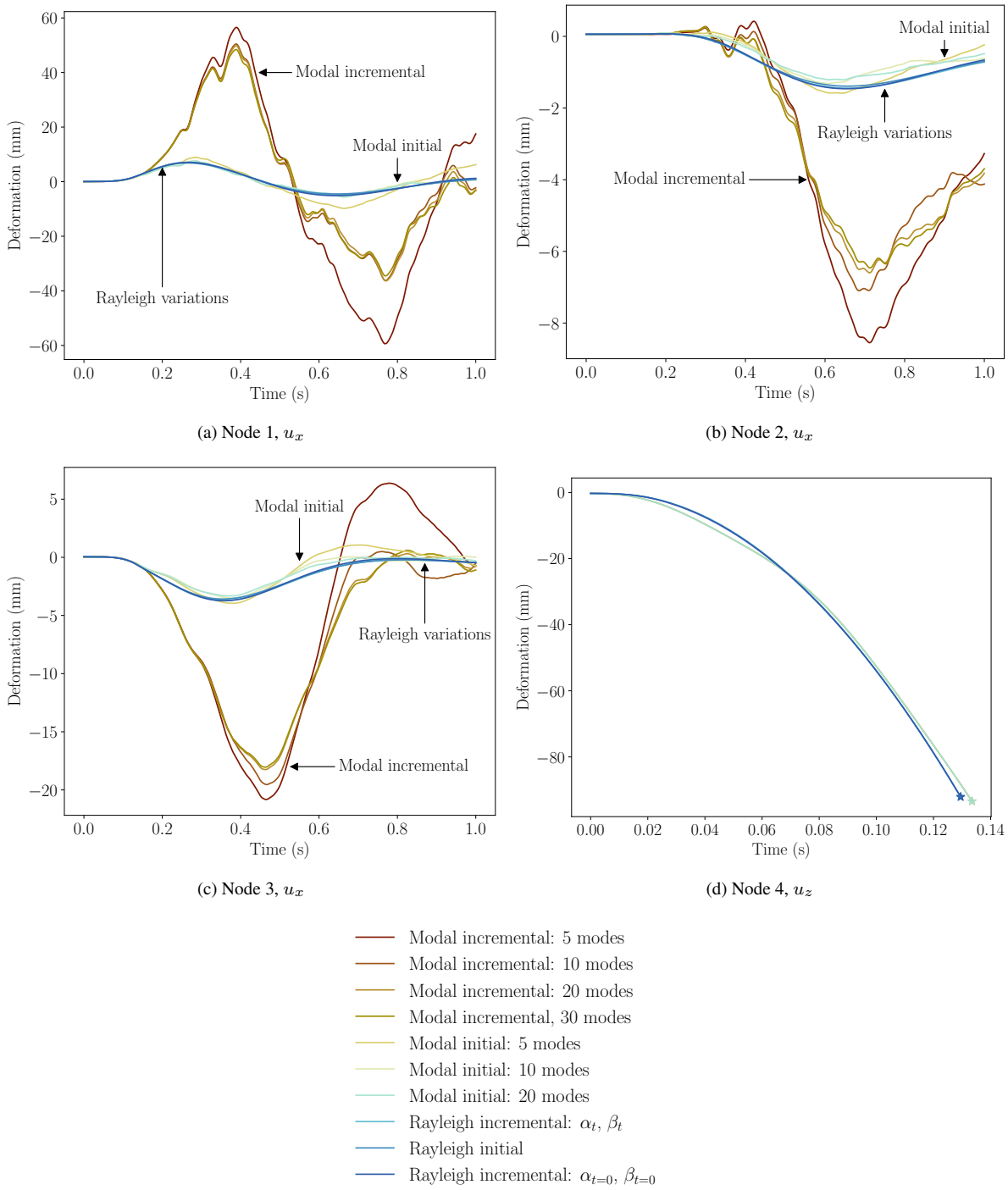

(a) Node 1, u_x

(b) Node 2, u_x

(c) Node 3, u_x

(d) Node 4, u_z

Figure 6: Nodal displacements for the different damping models.

Table 2 shows the root-mean-square deviation RMSD and normalized root-mean-square deviation NRMSD between the different damping models. As observed in Figure 6, the differences between the different Rayleigh damping models are quite small, with an RMSD less than 0.32. Similarly, the RMSD between the different Rayleigh damping models and the initial modal damping model is also of the same magnitude of around 0.55. The large dissimilarities between the incremental modal damping model and the other models result in an RMSD of

NRMSD (RMSD)		R_{in} $\alpha_{t=0}$, $\beta_{t=0}$	R_{inc} $\alpha_{t=0}$, $\beta_{t=0}$	R_{inc} α_t, β_t	M_{in}	M_{inc}
R_{in}	$\alpha_{t=0}$, $\beta_{t=0}$	0	1.14 (0.32)	0.54 (0.15)	1.87 (0.52)	68.82 (19.03)
R_{inc}	$\alpha_{t=0}$, $\beta_{t=0}$	1.14 (0.32)	0	0.92 (0.19)	2.73 (0.57)	89.84 (18.90)
R_{inc}	α_t, β_t	0.54 (0.15)	0.92 (0.19)	0	2.11 (0.55)	73.09 (18.92)
M_{in}		1.87 (0.52)	2.73 (0.57)	2.11 (0.55)	0	8.56 (19.17)
M_{inc}		68.82 (19.03)	89.84 (18.90)	73.09 (18.92)	8.56 (19.17)	0

Table 2: Root-mean-square deviation RMSD and normalized root-mean-square deviation NRMSD in parenthesis.

around 19, which is over 30 times higher than the RMSD between the other models.

For conventional nonlinear response history analyses without the separation and detachment of elements, modal damping is superior to Rayleigh damping [1, 11]. On this basis, it is believed that its incremental version offers the highest precision of the different damping models presented in this paper. With incremental modal damping, the damping model can to represent the changes in the mass **m**, stiffness **k**, and mode shapes ϕ_n throughout a progressive collapse. If the time steps Δt are small enough, the deformations from a time t_i to t_{i+1} are small, changes in stiffness can be reasonably idealized as linear, and the mode shapes do not change significantly. Therefore, the assumptions of modal analysis are not violated.

4.4 Issues with damping in progressive collapse

Although incremental modal damping may offer the highest precision of the different damping models in this paper, there is still an intrinsic problem with equivalent viscous damping ζ_{eq} for inelastic structures, and especially for structures undergoing a progressive collapse. Regardless of the damping models presented in this paper, the equivalent viscous damping ζ_{eq} was calibrated for a certain deformation level. Here, it was calibrated for an ultimate rotation θ_u of $3\theta_y$. The maximum vertical deflections u_z in the analyses conformed well to an ultimate rotation θ_u of $3\theta_y$. However, the calibrated equivalent viscous damping ζ_{eq} was only appropriate for the most deformed connections in the immediate vicinity of the removed column. The other connections further away from the removed column did not undergo nearly as large deformations. Therefore, the calibrated equivalent viscous damping ζ_{eq} was not appropriate for much of the structure. Because of this, the accuracy of the response history would deteriorate with the time. It is also possible to choose a value of the equivalent viscous damping ζ_{eq} that averages the damping of the entire structure. However, this approach is fraught with similar issues, where the equivalent viscous damping is incorrectly modeled everywhere.

To increase the accuracy of the damping modeling, there are essentially two approaches. The first approach is to model the hysteresis of the different members explicitly in the model with lumped or distributed plasticity. By modeling the hysteresis directly, the damping of the modeled members would have the highest precision. However, this approach may lead to excessive computation times and convergence problems if the members with hysteresis experiences segments of zero stiffness. Moreover, most hysteretic models are phenomenological and rely on physical tests for their calibration. This means that it is difficult to generalize the hysteretic models to all structural components.

The second approach is to calibrate and implement equivalent viscous damping ζ_{eq} for each member, which contributes significantly to the damping of the structure. Because the modal damping models rely on the mode shape of the whole structure, these models cannot be used.

Alternative damping models such as Rayleigh damping or stiffness-proportionate damping could be used, especially in lumped plasticity approaches where the plasticity is concentrated in members with nearly zero mass. However, these alternative damping models would inherit the same weaknesses as Rayleigh damping, such as spurious damping forces and near-infinite damping for high frequencies. Additionally, the calibration of the equivalent viscous damping ζ_{eq} for each component would be a tedious iterative process with its own uncertainties. This would lead to the need to do multiple analyses to find the appropriate equivalent viscous damping ζ_{eq} for all the relevant components of the structure.

Regardless of the two approaches, an appropriate amount of equivalent viscous damping ζ_{eq} would also need to be implemented to account for other sources of damping in the structure. These may stem from friction, non-load-bearing members, furniture and appliances, and more. The ideal approach to model damping in a structure undergoing a progressive collapse would be the explicit modeling of hysteresis in the connections, as well as a service-level equivalent viscous damping ζ_{eq} in the form of incremental modal damping. The service-level equivalent viscous damping ζ_{eq} can be adopted from any forced or ambient vibration test of similar structures in their elastic range, which is typically a few percent.

5 CONCLUSIONS

This paper presented different equivalent viscous damping models and discussed their applicability for nonlinear response history and progressive collapse analyses. Initial and two versions of incremental Rayleigh damping were assessed, besides initial and incremental modal damping. These damping models were implemented in a recently developed nonlinear parametric model for progressive collapse analysis. To compare the damping models in a progressive collapse, a symmetrical timber frame subjected to the removal of an edge column was analyzed. The timber frame comprised four bays and storeys with laterally loaded timber connections with dowel-type fasteners, and the equivalent viscous damping was estimated from a newly developed multi-scale hysteretic model for such timber connections.

The results showed that the response histories followed the same trend, with one positive and negative peak. For the initial modal damping and the Rayleigh damping models, the response histories were similar and high-frequency responses were damped out. However, the incremental modal damping model resulted in peak amplitudes that were in the order of five times higher than the other damping models. It also showed high-frequency response and the peaks occurred later. If the objective is to assess the structure until the first failure, the damping model is not critical. For this purpose, one of the incremental Rayleigh damping models may be used because of their computational efficiency. If the objective is to assess a progressive collapse past the first failure, the damping model may heavily influence the structural response. For this, the incremental modal damping model is recommended.

The best representation of the damping in an inelastic response history analysis is to model the hysteresis explicitly in the materials of the structure in a lumped or distributed plasticity approach. This should be combined with service-level equivalent viscous damping to account for other sources of damping. Further research is necessary to quantify the accuracy gains between the explicit modeling of hysteresis and equivalent viscous damping models, as well as the appropriate amount of service-level equivalent viscous damping.

REFERENCES

[1] A.K. Chopra, F. McKenna, Modeling viscous damping in nonlinear response history analysis of buildings for earthquake excitation. *Earthquake Engineering & Structural Dynamics*, **45**, 193–211, 2016.

[2] M.A. Bezabeh, G.T. Bitsuamlak, S. Tesfamariam, Nonlinear dynamic response of single-degree-of-freedom systems subjected to along-wind loads. I: Parametric study. *Journal of Structural Engineering*, **147**(11), 2021.

[3] G. Kaewkulchai, E.B. Williamson, Modeling the impact of failed members for progressive collapse analysis of frame structures. *Journal of Performance of Constructed Facilities*, **20**(4), 375–383, 2006.

[4] C. Viau, G. Doudak, Dynamic analysis methods for modelling timber assemblies subjected to blast loading. *Engineering Structures*, **233**, 2021.

[5] J.A.J. Huber, M. Ekevad, U.A. Girhammar, S. Berg, Structural robustness and timber buildings - a review. *Wood Material Science & Engineering*, **14**(2), 107–128, 2019.

[6] F.A. Charney, Unintended consequences of modeling damping in structures. *Journal of Structural Engineering*, **134**(4), 581–592, 2008.

[7] M.J.N Priestley, G.M. Calvi, M.J. Kowalsky, Direct displacement-based seismic design of structures. *2007 New Zealand Society for Earthquake Engineering Conference (2007 NZSEE)*, New Zealand, 2007.

[8] A.A. Correia, J.P. Almeida, R. Pinho, Seismic energy dissipation in inelastic frames: Understanding state-of-the-practice damping models. *Structural Engineering International*, **23**(2), 148–158, 2013.

[9] J.F. Hall, Problems encountered from the use (or misuse) of Rayleigh damping. *Earthquake Engineering & Structural Dynamics*, **35**, 525–545, 2006.

[10] J.F. Hall, Performance of viscous damping in inelastic seismic analysis of moment-frame buildings. *Earthquake Engineering & Structural Dynamics*, **47**, 2756–2776, 2018.

[11] X. Qian, A.K. Chopra, F. McKenna, Modeling viscous damping in nonlinear response history analysis of steel moment-frame buildings: Design-plus ground motions. *Earthquake Engineering & Structural Dynamics*, **50**, 903–915, 2021.

[12] A.S. Cao, L. Esser, B. Glarner, A. Frangi, A nonlinear dynamic model for collapse investigations in tall timber buildings - Preliminary results. *World Conference on Timber Engineering 2023 (WCTE2023)*, Oslo, Norway, June 19-22, 2023.

[13] A.S. Cao, A. Frangi, Mixed element method for progressive collapse analysis: Method description and verification. F. Di Trapani ed. *Proceedings of Eurasian OpenSees Days 2022 (OpenSeesDays2022)*, Torino, Italy, July 7-8, 2022.

[14] A.S. Cao, P. Palma, A. Frangi, Multi-scale hysteretic model of laterally loaded timber connections with dowel-type fasteners. *World Conference on Timber Engineering 2023 (WCTE2021)*, Santiago, August, July 9-12, 2021.

[15] A.S. Cao, M. Lolli A. Frangi, Pendulum impact hammer tests on spruce GLT - Preliminary results B.H.V. Topping, J. Kruis eds. *Proceedings of the Fourteenth International Conference on Computational Structures Technology (CST2022)*, Montpellier, France, August 23-25, 2022.

[16] A.S. Cao, P. Palma, A. Frangi, Multi-scale hysteretic model of laterally loaded timber connections with dowel-type fasteners. J.F. Silva Gomes ed. *20th International Conference on Experimental Mechanics (ICEM20)*, Porto, Portugal, July 2-7, 2023.

[17] European Committee for Standardization, *EN 1990:2002. Eurocode - Basis of structural design*. European Committee for Standardization (CEN), 2002.

[18] European Committee for Standardization, *EN 1991-1-1:2002. Eurocode 1: Actions on structures - Part 1-1: General actions - Densities, self-weight, imposed loads for buildings*. European Committee for Standardization (CEN), 2002.

[19] European Committee for Standardization, *EN 14080:2013. Timber structures - Glued laminated timber and glued solid timber - Requirements*. European Committee for Standardization (CEN), 2013.

[20] European Committee for Standardization, *EN 1995-1-1:2004. Design of timber structures - Part 1-1: General - Common rules and rules for buildings*. European Committee for Standardization (CEN), 2004.

[21] International Organization for Standardization, *ISO 10137:2007. Bases for design of structures - Serviceability of buildings and walkways against vibrations*. International Organization for Standardization (ISO), 2007.

[22] European Committee for Standardization, *EN 1991-1-4:2005. Actions on structures - Part 1-4: General actions - Wind actions*. European Committee for Standardization (CEN), 2005.

[23] S. Schilling, P. Palma, R. Steiger, A. Frangi, Probabilistic description of the mechanical properties of glued laminated timber made from softwood. R. Görlacher Ed. *Proceedings of the International Network on Timber Engineering Research, INTER, Meeting 54 (INTER 2021)*, Online, August 16-19, 2021.

[24] Joint Committee on Structural Safety, *JCSS - Probabilistic Model Code: Part III Resistance Models - Steel*. Joint Committee on Structural Safety (JCSS), 2000.

[25] European Committee for Standardization, *EN 1991-1-7:2006. Actions on structures - Part 1-7: General actions - Accidental actions*. European Committee for Standardization (CEN), 2006.

[26] J. Munch-Andersen, P. Dietsch, Robustness of large-span timber roof structures - Two examples. *Engineering Structures*, **33**(11), 3113–3117, 2011.